Biosensors and Bioelectronics 68 (2015) 521–528

Contents lists available at ScienceDirect

Biosensors and Bioelectronics

journal homepage: www.elsevier.com/locate/bios

Diamond nanoparticles based biosensors for efficient glucose and lactate determination

M. Briones [a], E. Casero [a,*], M.D. Petit-Domínguez [a], M.A. Ruiz [a], A.M. Parra-Alfambra [a], F. Pariente [a], E. Lorenzo [a,b], L. Vázquez [c]

[a] Departamento de Química Analítica y Análisis Instrumental, Facultad de Ciencias, Campus de Excelencia de la Universidad Autónoma de Madrid, c/ Francisco Tomás y Valiente N°7, 28049 Madrid, Spain
[b] Instituto Madrileño de Estudios Avanzados (IMDEA)-Nanoscience, Faraday 9, Campus Cantoblanco-UAM, 28049 Madrid, Spain
[c] Instituto de Ciencia de Materiales de Madrid (CSIC), Campus de Excelencia de la Universidad Autónoma de Madrid, c/Sor Juana Inés de la Cruz N°3, 28049 Madrid, Spain

ARTICLE INFO

Article history:
Received 17 November 2014
Received in revised form
15 January 2015
Accepted 19 January 2015
Available online 20 January 2015

Keywords:
Diamond nanoparticles
Lactate biosensor
Glucose biosensor
Electrochemical techniques
Atomic force microscopy

ABSTRACT

In this work, we report the modification of a gold electrode with undoped diamond nanoparticles (DNPs) and its applicability to the fabrication of electrochemical biosensing platforms. DNPs were immobilized onto a gold electrode by direct adsorption and the electrochemical behavior of the resulting DNPs/Au platform was studied. Four well-defined peaks were observed corresponding to the DNPs oxidation/reduction at the underlying gold electrode, which demonstrate that, although undoped DNPs have an insulating character, they show electrochemical activity as a consequence of the presence of different functionalities with unsaturated bonding on their surface. In order to develop a DNPs-based biosensing platform, we have selected glucose oxidase (GOx), as a model enzyme. We have performed an exhaustive study of the different steps involved in the biosensing platform preparation (DNPs/Au and GOx/DNPs/Au systems) by atomic force microscopy (AFM), field emission scanning electron microscopy (FE-SEM) and cyclic voltammetry (CV). The glucose biosensor shows a good electrocatalytic response in the presence of (hydroxymethyl)ferrocene as redox mediator. Once the suitability of the prototype system to determine glucose was verified, in a second step, we prepared a similar biosensor, but employing the enzyme lactate oxidase (LOx/DNPs/Au). As far as we know, this is the first electrochemical biosensor for lactate determination that includes DNPs as nanomaterial. A linear concentration range from 0.05 mM to 0.7 mM, a sensitivity of 4.0 μA mM^{-1} and a detection limit of 15 μM were obtained.

1. Introduction

In recent years, a wide range of carbon nanomaterials has been explored as potential based platforms for developing biosensing systems. Among them, carbon nanotubes and graphene are the most employed due to their unique mechanical, electrical, thermal and optical properties (Merkoçi et al., 2005; Pumera, 2009; Yang et al., 2010; Kochmann et al., 2012). Recently, a new member of the carbon nanomaterials family, denoted as diamond nanoparticles (DNPs), has gained attention since it presents some additional advantages compared to other carbon nanomaterials such as an excellent biocompatibility, a noncytotoxic nature, a narrow size distribution and a moderate price since it can be produced at large-scale by detonation methods. Furthermore, as a consequence of the purification procedures employed after fabrication, DNPs possess several oxygenated functional groups on its surface, including hydroxyl and carboxyl groups, which facilitate the immobilization of biomolecules. Due to this interesting surface chemistry, it has been possible to conjugate DNPs with peptide nucleic acids (Gaillard et al., 2014), anticancer-drugs (Li et al., 2010), antibodies (Zhang et al., 2014) and proteins such as glucose oxidase (Zhao et al., 2006), hemoglobin (Zhu et al., 2007), alcohol dehydrogenase (Nicolau et al., 2012), cytochrome c (Chang and Lora Huang, 2004), lysozyme (Chang et al., 2007), and bovine seroalbumine (Wang et al., 2011). The possibility of immobilizing a wide variety of biomolecules in conjunction with the excellent properties mentioned above, makes DNPs good candidates for several biomedical applications such as protein separation, drug delivery and biosensing (Man and Ho, 2012; Puzyr et al., 2007). Particularly, in the field of biosensors, DNPs have been incorporated in analytical platforms for glucose (Zhao et al., 2006),

* Corresponding author.
E-mail address: elena.casero@uam.es (E. Casero).

http://dx.doi.org/10.1016/j.bios.2015.01.044
0956-5663/

alcohol (Nicolau et al., 2012) or nucleic acids (Gaillard et al., 2014) determination. Furthermore, it has been proven that DNPs are able to promote direct electron transfer between redox enzymes and the underlying electrode (Zhu et al., 2007).

Concerning the employment of DNPs for electrochemical biosensors, it should be highlighted that, in contrast with the advantages mentioned above, undoped diamond has an insulating character, with a band gap of 5.47 eV (Clark et al., 1964). An approach commonly used to overcome this problem consists in the employment of diamond doped with different elements such as boron, as a way to increase its conductivity (Cunci and Cabrera, 2011). However, several studies have shown that, despite the great bandgap value, undoped diamond can also be considered as a potential material for electrode fabrication. In this sense, several strategies to incorporate DNPs into electrodes can be found in the literature. In one of the first reports concerning the employment of DNPs as electrode (Novoselova et al., 2004), they were sintered at high pressure and temperature to form pellets. In this case, the resistance of the powder was so high that the electrochemical response of a redox probe in solution was superimposed on a linearly sloping background, similar to that obtained for a resistor. However, some later reports show that undoped DNPs immobilized onto an electrode surface enhance the electrochemical response of different redox probes in solution, such as $Fe(CN)_6^{3-/4-}$, $Ru(CN)_6^{3-/4-}$, $Ir(Cl)_6^{2-/3-}$, $Ru(NH_3)_6^{3+}$ and (hydroxymethyl)ferrocene (Holt et al., 2009; Holt, 2010; Scholz et al., 2011; Varley et al., 2014). According to these authors, the enhancement of the oxidation/reduction current is a consequence of i) electron transfer between diamond nanoparticles and the redox probe in solution, evidencing the existence of DNPs surface redox states at given pH-dependent potentials and ii) electron transfer mediated by the redox probe adsorbed onto the diamond nanoparticles surface. The surface redox states are related to the presence of a considerable number of functional groups at the DNPs surface, as a consequence of the synthesis procedure and the subsequent purification methods. Therefore, although bulk diamond is known to be a good insulator, its properties cannot be generalized at the nanoscale since new phenomena may appear. In this case, it can be assumed that although DNPs are non-conducting in a conventional manner, they do display redox activity.

In this article, we address some issues concerning the employment of diamond nanoparticles as a promising nanomaterial for electrochemical biosensing applications. As a model system, we develop a DNPs-based biosensing platform employing glucose oxidase. This first prototype was employed to perform an exhaustive study of the system, helping us to extend further the acquired knowledge to the development of lactate oxidase biosensors. In a first step, we have immobilized DNPs on a gold electrode and we have characterized the resulting surface by atomic force microscopy (AFM), field emission scanning electron microscopy (FE-SEM) and cyclic voltammetry (CV). These studies demonstrate the suitability of a direct adsorption strategy to immobilize DNPs onto metallic surfaces. Afterwards, glucose oxidase (GOx) was directly adsorbed onto the DNPs modified gold electrode. The morphology of GOx/DNPs/Au surfaces was studied by AFM and FE-SEM, the enzyme layer thickness was determined by force spectroscopy measurements and the electrochemical response towards a redox probe in solution was obtained. Finally, the response of the biosensor towards glucose was studied. Once the suitability of the prototype system to determine glucose was verified, in a second step, we prepared a new biosensor based on the same procedure but employing the enzyme lactate oxidase. To our knowledge, this is the first electrochemical biosensor for lactate determination that includes DNPs as nanomaterial.

2. Experimental section

2.1. Materials

Diamond nanoparticles (DNPs) are obtained from SkySpring Nanomaterials, Inc. (Product 0512HZ) (Houston, TX). Lactate oxidase (LOx, EC 232-841-6 from Pediococcus species) and glucose oxidase (GOx, EC 1.1.3.4 from *Aspergillus niger*) lyophilized powder containing 41 U/mg solid and 15,200 U/g solid, respectively were obtained from the Sigma Chemical Co. (St. Louis, MO). Stock solutions were prepared dissolving 1.3 mg of the LOx lyophilized powder in 250 μL of 0.1 M phosphate buffer solution (pH=7.0) and 7.5 mg of the GOx lyophilized powder in 250 μL of 0.1 M acetate buffer solution (pH=4.5), aliquoted (10 μL) and stored at −30 °C. Under these conditions, the enzymatic activity remains stable for several weeks. L-(+)-lactic acid lithium salt 97%, D-(+)-Glucose (99.5%), acetaminophen, uric acid, ascorbic acid and (hydroxymethyl)ferrocene (HMF) were obtained from Aldrich Chemical Co. (Milwaukee, WI). Sodium phosphate and sodium acetate (Merck) were employed for the preparation of buffer solutions. Other chemicals used in this work were reagent grade quality and used as received without additional purification steps. Water was purified with a Millipore Milli-Q-System. All solutions were prepared just prior to use.

2.2. Experimental techniques

The Atomic Force Microscopy (AFM) data were obtained with a Nanoscope IIIa equipment (Veeco). For those studies performed in air, silicon tips, with a nominal spring constant in the 1–5 N/m range and a nominal tip radius of 8 nm (Bruker) were employed. For those measurements performed in buffer conditions oxide sharpened silicon nitride tips, with a spring constant of 0.24 N/m and nominal tip radius of 10 nm, were used. All images have been taken in the intermittent contact mode.

We have also performed force spectroscopy measurements by recording the approach force curves where the cantilever deflection is registered as a function of the vertical *z*-displacement. Under this configuration, the tip is at a fixed point over the surface and approaches it vertically. Typically, when the tip is far from the surface there is no any deflection (zero force) until the tip contacts the surface. At this point, if the surface is more rigid than the cantilever, such as nanodiamond, there is a new region in the force curve characterized by a linear dependence, with slope one, of the deflection with the *z*-displacement. This behavior is due to the fact that the tip does not indent the rigid surface and, therefore, the whole *z*-displacement is transferred as deflection to the tip. In contrast, when a soft material, such as an enzyme, is sampled the tip does indent it to some extent. This fact is reflected in the force curve by the appearance of curved regions (with smaller slopes) once the tip contacts the surface. In addition, the force curve is shifted with respect to that obtained on the rigid surface in such way that for a given deflection (i.e. force) this horizontal shift corresponds to the indentation. Eventually, if the soft layer is thin enough the underlying hard substrate is reached and the linear regime with slope one is attained. In this case, the horizontal gap measured for the same force between both linear regions is an estimation of the thickness of the soft layer deposit on top of the hard surface.

The field emission scanning electron microscope (FE-SEM) was an ISI (DS-130C). Measurements were carried out under high vacuum conditions.

Electrochemical measurements were carried out with an Ecochemie Autolab PGSTAT12 system (Utrecht, The Netherlands) employing a three-compartment cell with a working gold electrode and a platinum wire as counter electrode. All potentials were

reported with respect to a Ag/AgCl reference electrode. All solutions were deaerated with nitrogen gas before use, keeping the gas flow over the solutions during experiments.

2.3. Procedures

2.3.1. Preparation of the samples used for AFM and FE-SEM measurements

Surfaces employed for these measurements consist of glass substrates (1.1 cm × 1.1 cm) covered with a chromium layer (1–4 nm thick) on which a gold layer (200–300 nm thick) was deposited (Arrandee Co. Werther, Germany). Prior to use, gold surfaces were annealed for 2 min in a gas flame in order to obtain Au (1 1 1) terraces.

Samples for AFM and FE-SEM morphological measurements were prepared by deposition of 100 μL of a suspension of DNPs in water (1 mg/mL) on gold surfaces and allowing them to air-dry. Then, AFM samples were measured both in air and in buffer conditions (phosphate buffer solution 0.1 M, pH 7) by AFM in the intermittent contact mode.

Samples for determining the average diameter of diamond nanoparticles by AFM were prepared in a different way due to the great tendency of DNPs to agglomerate (Kulakova, 2004). In this case, it is necessary to deposit single nanoparticles on a flat substrate in order to obtain their height distribution unambiguously. The same flame-annealed gold substrates used in the other AFM studies were first used, but they did not prove to be suitable for this study since the stepped morphology and roughness of the bare flame-annealed gold substrate make difficult to unambiguously measure the diameter of isolated DNPs. Therefore, a different substrate, silicon, was chosen only for this study due to its extreme flatness since its surface roughness is just 0.2 nm. Silicon substrates were located at the bottom of a vase containing the suspension of DNPs in water (1 mg/mL) and sonicated during 1 h. In this way, the aggregates, thanks to the shaking process, were able to disaggregate to some extent (Krüger et al., 2005), leading to deposits on the substrate with both aggregates and isolated DNPs. Afterwards, the DNPs modified surface was dried under nitrogen and measured by AFM in the intermittent contact mode. Note that to avoid tip convolution effects, the size distribution was obtained by measuring the height of the isolated DNPs.

2.3.2. Preparation of the electrochemical biosensing platforms

Prior to each experiment, gold electrodes were polished with 1 μm diamond paste (Buehler) and rinsed with water. Then, they were conditioned to obtain a proper baseline and stable response by holding the potential at +2.0 V for 5 s in 0.1 M H_2SO_4 and then at −0.35 V for 10 s. Afterwards, potential cycling from −0.20 to +1.5 V at 5 V/s for 2 min was performed. Finally, the cyclic voltammogram characteristic of a clean polycrystalline gold electrode was recorded (from −0.2 to +1.5 V) at 100 mV/s. The electrode was subsequently rinsed with water, air-dried, and modified with 5 μL of the DNPs suspension. Finally, the electrochemical biosensing platforms, GOx/DNPs/Au and LOx/DNPs/Au, were fabricated by placing 5 μL of the corresponding enzyme stock solution (GOx or LOx) onto the DNPs/Au electrode surface. After air-dried, the modified electrodes were washed with water to remove any weakly bound material.

3. Results and discussion

3.1. Determination of the average DNPs diameter

Fig. 1A shows a characteristic AFM image of the DNPs modified Si morphology. Different nanoparticles can be observed scattered over the flat silicon surface, but in several places aggregates of nanoparticles have also been found. In order to reliably estimate the nanoparticle diameter, we have measured the height of those imaged structures that did not show any evidence of aggregation. In this process, the corresponding phase shift image is very useful in order to detect such aggregates. We analyzed the height rather than the lateral size of the structures because the latter is indeed affected by tip convolution effects. After analyzing more than 300 nanoparticles, we obtained the histogram displayed in Fig. 1B. These data lead to an average height (diameter) value of $<h> = 9 \pm 3.6$ nm.

3.2. Morphological characterization of DNPs/Au and GOx/DNPs/Au systems

For developing the biosensing platform, the first step consists of nanostructuring a bare gold electrode with diamond nanoparticles (DNPs/Au), following the procedure described in the experimental section. AFM imaging of the DNPs deposit in air was a

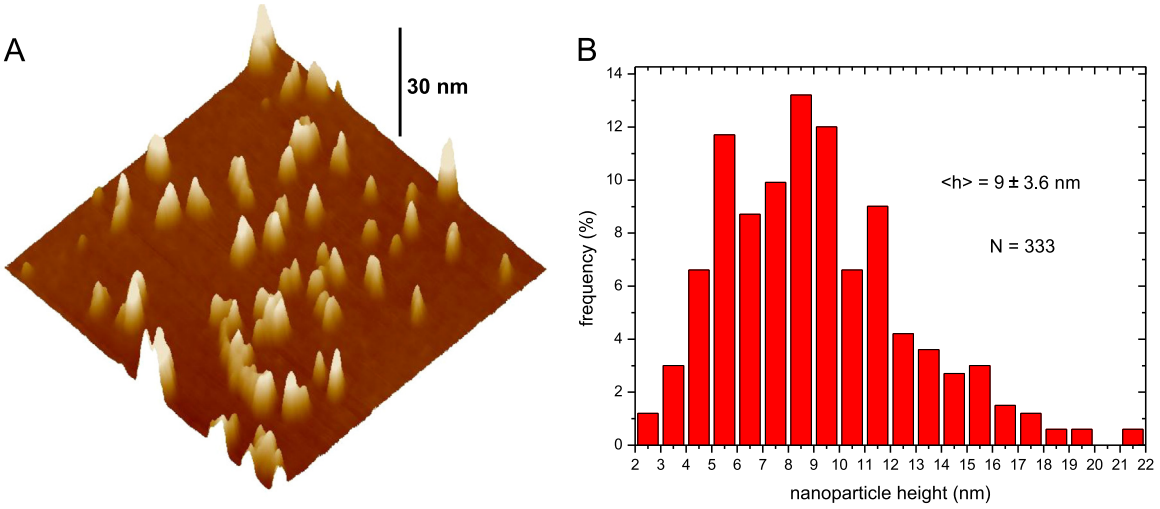

Fig. 1. (A) 500 × 500 nm^2 AFM image taken in the intermittent contact mode in air of a silicon surface on which DNPs have been deposited following a given procedure (see Section 2) to prevent aggregation. (B) Histogram of the height measured by AFM on 333 diamond nanoparticles deposited on a silicon surface. The average value is 9 ± 3.6 nm.

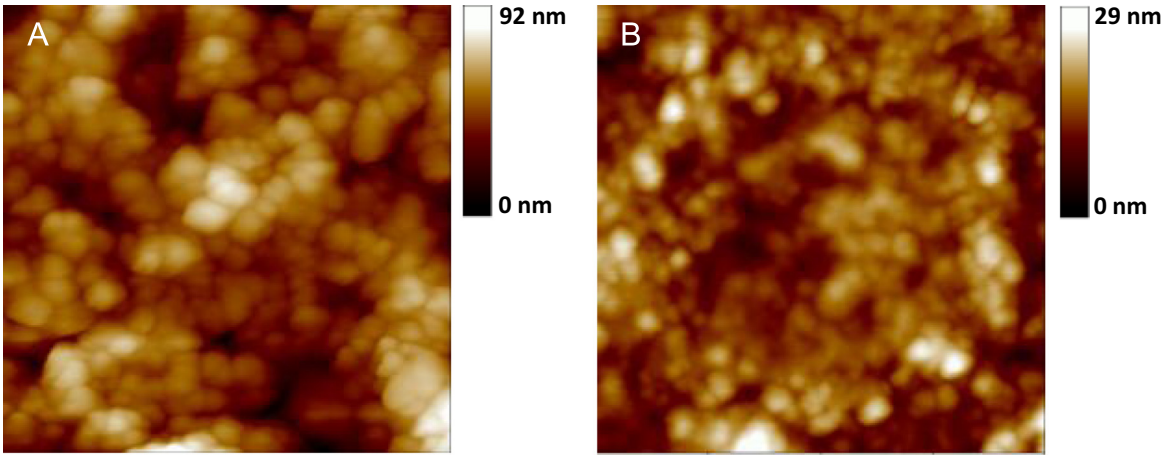

Fig. 2. 400×400 nm^2 intermittent contact mode AFM images taken under air conditions of (A) DNPs/Au and (B) GOx/ DNPs /Au systems.

difficult task because of its extreme hardness. When standard silicon tips with spring constants around 40 N/m were employed, the tip became blunted from the very first measurements stages, even when low free amplitude conditions were used. Thus, the imaged structures were largely affected by the associated tip convolution problems. Therefore, much softer cantilevers were used in order to apply lower forces with the aim of preserving the tip status. Under these conditions, images as such displayed in Fig. 2A were obtained on the DNPs deposit. The first aspect to highlight is the relative large surface roughness of the deposit, with a surface roughness of 12 nm. This fact poses an additional problem to reliably estimate the DNPs size as tip convolution effects become enhanced for those structures located at the top of the surface protrusions. In these spots, lateral sizes of 30 nm can be measured, whereas, at the depressions, structures as small as 10 nm in size can be observed. In any case, it should be reminded that tip convolution effects would be present in the whole image. Furthermore, the tendency of the diamond nanoparticles to aggregate can also lead to larger structures. However, it is worth noting the neat contour of the nano-granular structures.

In a further step, we proceeded to visualize by AFM, also in ambient conditions, the diamond nanoparticles deposit with the

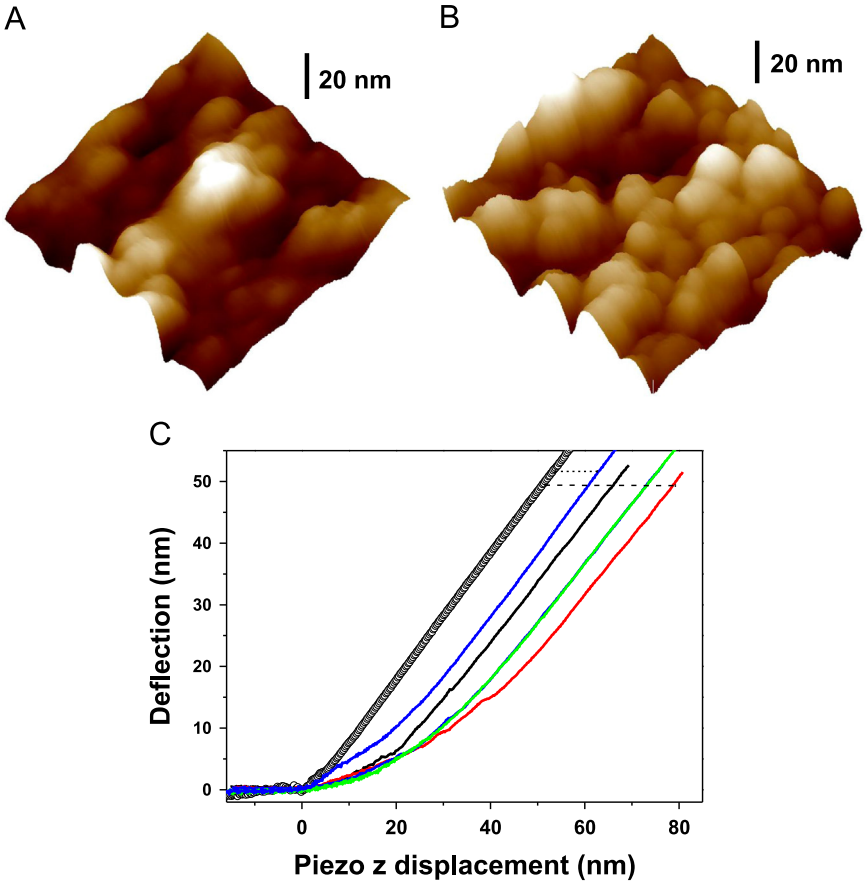

Fig. 3. 127×127 nm^2 intermittent contact mode AFM image taken under buffer conditions of (A) DNPs/Au and (B) GOx/DNPs/Au systems. (C) Characteristic force curves obtained on the DNPs/Au surface (open circles) and on different locations of the GOx/DNPs/Au sample (solid lines). For a given deflection the indentation on the GOx structures is measured as the lateral shift of the corresponding GOx curve with respect to the DNPs curve (horizontal dashed lines).

enzyme structures (GOx/DNPs/Au). The typical image that we obtained for GOx is shown in Fig. 2B. The image shows certain likeness to the previous one. However, now the granular structures are not as neat as in the DNPs case. In fact, the image is somehow blurred with respect to that obtained on the DNPs surface. Again, tip convolution effects are present, particularly in those structures located at the higher spots. Structures as large as 30 nm are also measured but smaller ones, in the 6–10 nm range, are detected as well. It is worth mentioning that now the surface roughness is smaller, close to 4 nm, which can be due to the smoothening of the DNPs surface by the GOx deposit.

Both samples were also imaged by FE-SEM (see Supplementary information, Fig. S1). Despite the low contrast obtained, likely due to the smooth morphology and low atomic number of the deposits, the images show clear differences. Thus, while nanodiamond structures are clearly resolved in the DNPs/Au only some of them are resolved for GOx/DNPs/Au. In this last system, dark patches, probably associated with GOx deposits, are also imaged. These dark zones become damaged under irradiation at high beam energy/current or prolonged exposure time, which indicates their soft nature.

In order to try to better characterize these two samples, we have attempted to perform the AFM measurements under buffer conditions and with softer cantilevers. Fig. 3A shows a high resolution image of the DNPs sample taken under these conditions.

Despite the problems due to the rough morphology and tip convolution effects, lateral sizes of the nanoparticles as small as 6 nm can be measured, together with larger values in the 10–15 nm range. The corresponding image for the GOx/DNPs/Au sample is shown in Fig. 3B. The main difference with respect to that obtained on DNPs/Au (Fig. 3A) is that the image is still somehow blurred and the contours of the nanometric structures are not as well defined as in the case of the diamond nanoparticles. Regarding the lateral size of the structures a similar range of values, from 6 nm to 15 nm, is found. This fact is not surprising since the basic structures of both systems, i.e., the diamond nanoparticles and the GOx molecules have quite similar sizes. Moreover, the difficulties to distinguish them even become enhanced by the tip convolution effects.

Accordingly, we have used other strategy to reveal their differences. Thus, we have measured several force curves when the samples were imaged under buffer conditions. As the DNPs surface is much more rigid than that of the GOx molecules, certain differences should arise when comparing their characteristic force curves (Fig. 3C). In this figure the typical curves obtained on the DNPs/Au and the GOx/DNPs/Au systems are displayed. Both present the zero deflection region when the tip is far from the surface. That one taken on DNPs/Au shows, once the tip contacts the surface, the straight region with slope one. This region is reached for the GOx/DNPs/Au curves for larger *z*-displacements, particularly after a first marked curved region (smaller slope) immediately after the tip contacts the surface. This zone displaying a curved shape, or smaller slopes than one, corresponds to the soft GOx deposit sampled by the tip. As commented above, the indentation done by the tip on these soft structures corresponds to the horizontal gap between the DNPs/Au and GOx/DNPs/Au curve for the same deflection. In the cases displayed in Fig. 3C all the GOx/DNPs/Au curves do reach finally the straight regime with slope one, which indicates that the underlying diamond nanoparticles surface has been reached. Thus, in these cases the lateral gap between the DNPs/Au and the GOx/DNPs/Au curves for high deflection values (marked by horizontal dashed lines) would correspond to the GOx layer thickness. For the curves displayed in Fig. 3C thickness values ranging from 9.5 nm to 18 nm are obtained. It should be noted that we have also measured force curves in which the straight line regime with slope one is not reached for the force range sampled. This means that thicker GOx deposits are also present. Therefore, these data indicate that GOx is deposited on the DNPs/Au surface with a variable thickness (from one monolayer to several layers). This fact agrees with the blurred and smoother morphology found in air (Fig. 2B) as compared with that measured on the DNPs/Au system (Fig. 2A).

3.3. Electrochemical characterization of DNPs/Au and redox-enzyme/DNPs/Au systems

As mentioned in the introduction, although undoped DNPs have an insulating character, they show electrochemical activity (Holt et al., 2009; Holt, 2010; Varley et al., 2014). This fact is a consequence of the presence of specific functionalities with unsaturated bonding on their surface, such as C=C and C=O. Thus, molecular orbitals of these functionalities overlap, leading to electronic states (π and π^*) whose energy values lie within the diamond band gap. The resulting energies of these discrete electronic states take different values depending on several factors including, for example, both the type of functionality and the number of neighboring atoms with different environments participating in the formation of the electronic states. Thus, DNPs present an unsaturated character since they have a great number of both unpaired electrons and unfilled electronic states, which can be oxidized or reduced depending on their potential relative to the underlying electrode or to a particular redox probe. Since different manufacturers use diverse purification procedures that result in different oxygenated functionalities at the DNPs surface, the redox states for each given DNPs system should be studied. In addition, other factors, such as the nature of the underlying electrode and the DNPs immobilization method employed, can be also relevant. The oxidation/reduction redox processes for our system (DNPs directly adsorbed onto a gold substrate employed as underlying electrode) are shown in Fig. 4A. This figure displays a differential pulse voltammogram (DPV) of a DNPs/Au electrode in PBS 0.1 M at pH 7. The background obtained for a bare gold electrode (before modification with the DNPs) in the same buffer solution has been subtracted in order to ensure that the response is due to the nanomaterial. In these conditions, four well-defined peaks are observed from −0.3 V to +0.7 V (at −0.22 V, +0.05 V, +0.23 V and +0.52 V) that correspond to oxidation/reduction of DNPs surface functionalities at the underlying gold electrode.

For a redox probe, such as HMF, the cyclic voltammetry at DNPs/Au nanostructured electrode (Fig. 4B, curve b) shows the typical redox response of the HMF(Fe^{II})/HMF(Fe^{III}) process in aqueous media at a formal potential of +0.27 V. Compared with the response of a bare gold electrode (Fig. 4B, curve a), the current intensity of both anodic and cathodic peaks is clearly enhanced. In particular, in the presence of DNPs, the oxidation and reduction currents are found to be enhanced about four-fold and two-fold, respectively. This current enhancement can be explained by considering that DNPs can cause an increment of the relative surface area as well as that they can undergo oxidation and reduction as a consequence of the existence of DNPs surface redox states. The catalytic feedback mechanism can be explained as follows: in the anodic scan of Fig. 4B (curve b), oxidation of HMF(Fe^{II}) to HMF(Fe^{III}) takes place over the gold surface. Subsequently, an electron transfer from DNPs surface to HMF(Fe^{III}) occurs, allowing that HMF(Fe^{III}) generated at the gold surface is rapidly reduced to HMF(Fe^{II}). As a consequence of this feedback mechanism, oxidation currents are enhanced. On the cathodic scan of Fig. 4B (curve b), the opposite process takes place enhancing the reduction currents. The proposed feedback mechanism is supported by the fact that, as can be observed in Fig. 4A, DNPs can be oxidized at a similar potential than that of HMF. Moreover, for DNPs/Au platform (Fig. 4B, curve b) a well-resolved, chemically irreversible peak

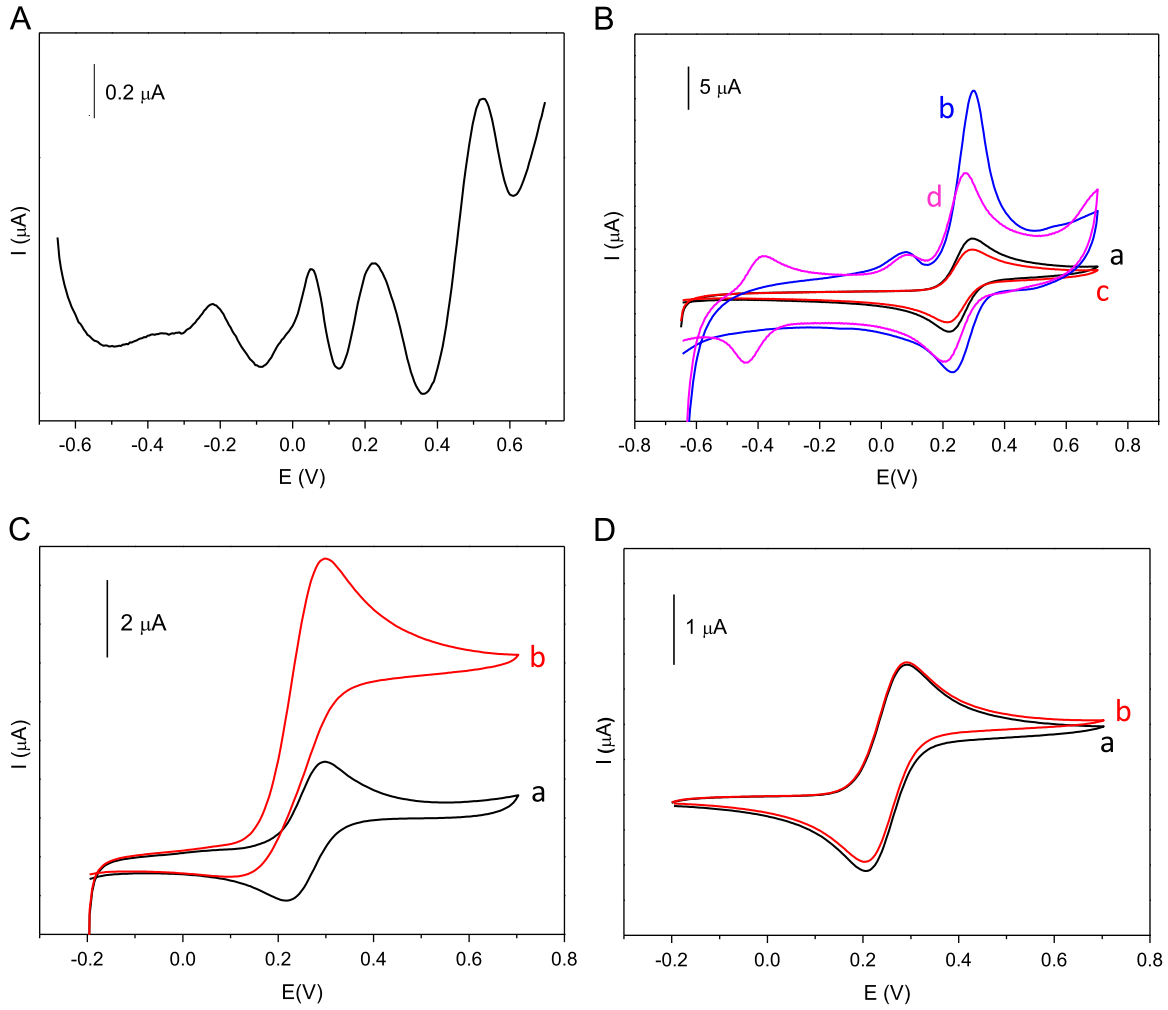

Fig. 4. (A) DPV of DNPs/Au in 0.1 M pH 7.0 phosphate buffer solution. Other conditions: scan rate 25 mV s^{-1}, pulse amplitude 50 mV and step potential 2 mV. (B) Cyclic voltammograms of bare gold (a), DNPs/Au (b), GOx/Au (c) and GOx/DNPs/Au (d) electrodes in 0.1 M pH 7.0 phosphate buffer solution containing 1 mM of HMF. Other conditions: scan rate 100 mV s^{-1}. (C, D) Cyclic voltammetric response for GOx/DNPs/Au and GOx/Au biosensors respectively, in contact with a 0.1 M phosphate buffer solution pH 7.0 containing 1.0 mM HMF in absence (curve a) and in presence (curve b) of 5 mM of glucose. Scan rate $\nu = 0.01$ V/s. All measurements were performed under nitrogen atmosphere.

appears close to the typical reversible wave of the HMF(Fe^{II})/HMF(Fe^{III}). Since this new peak (at a potential value of +0.10 V) does not appear in phosphate buffer without HMF (data not shown), it is not related with the DNP itself, but rather with processes involving HMF on its surface. This pre-peak can be explained by taking into account that HMF(Fe^{III}) can be adsorbed onto the DNPs modified surface. Since the redox potential of an adsorbed compound is not exactly the same than that of the same compound in solution, the pre-peak appears at a relatively lower potential than the main peak.

The electrochemical characterization of the biosensing platform (GOx/DNPs/Au) was performed under the same conditions. The resulting voltammogram (Fig. 4B, curve d) shows a new pair of redox peaks located at a formal potential of −0.4 V, which is consistent with the reversible oxidation–reduction of the $FAD/FADH_2$ of the enzyme according to

$$GOx(FAD) + 2e^- + 2H^+ \leftrightarrow GOx(FADH_2) \quad (1)$$

As can be anticipated, the formal potential of the redox couple was pH dependent (data not shown), with a slope of 64 mV per pH unit, which is very close to the Nernstian value of 59 mV for electrochemical processes involving the same number of protons and electrons, and is also in accord with Eq. (1). Moreover, a linear relationship is obtained between intensity current and scan rate (data not shown), indicating that process described in Eq. (1) is surface controlled.

In order to assess the influence of both enzyme and DNPs in this $FAD/FADH_2$ redox process, we compare the CV's obtained for: the biosensor GOx/DNPs/Au (Fig. 4B, curve d), a bare gold electrode (Fig. 4B, curve a), a DNPs/Au electrode (Fig. 4B, curve b) and a GOx/Au electrode (Fig. 4B, curve c). As can be observed, these three control experiments yielded featureless voltammograms in this region (around −0.4 V). Therefore, it is clear that the presence of DNPs is mandatory to obtain the redox peaks at −0.4 V, corresponding to the reversible oxidation–reduction of the $FAD/FADH_2$ prosthetic group. In this sense, it seems that DNPs are able to promote direct electron transfer between redox enzymes and the underlying electrodes. This fact has been previously described in the literature (Zhu et al., 2007). In order to confirm that the direct electron transfer is due to the presence of DNPs and not to the material of the underlying electrode, we have performed a similar experiment, but employing a glassy carbon electrode instead of a gold one, obtaining the same results (data not shown). A second remarkable feature for GOx/DNPs/Au cyclic voltammogram is that the current intensity of both anodic and cathodic peaks corresponding to HMF(Fe^{II})/HMF(Fe^{III}) process is clearly diminished with respect to DNPs/Au system. This can be due to the fact that the presence of GOx adsorbed onto the DNPs can obstruct

partially the electron transfer from DNPs surface to HMF, hindering the feedback mechanism and, therefore, diminishing the current intensity of both cathodic and anodic peaks of HMF redox couple. This behavior is also observed when the electrode employed for immobilizing the DNPs is glassy carbon instead of gold (data not shown).

Finally, the response of the GOx/DNPs/Au model biosensing platform towards glucose is studied. In presence of oxygen, GOx/DNPs/Au biosensor catalyzes the oxidation of glucose, generating hydrogen peroxide as one of the products of the reaction. Thus, the activity of the immobilized enzymes can be electrochemically detected by monitoring the H_2O_2 produced. However, since a high potential (around 0.5 V) is required for H_2O_2 amperometric detection (data not shown), this strategy is not reliable because it can be eventually affected by potential interfering species present in the sample, which could also become oxidized at this high potential. In order to overcome this problem, one of the most important strategies reported in the literature is based on the replacement of the natural electron acceptor (O_2) by an artificial mediator. From the studies described above and our previous experience with other oxidases (Barbadillo et al., 2009; Casero et al., 2013, 2014; Parra et al., 2006; Parra-Alfambra et al., 2011), we have selected the (hydroxymethyl)ferrocene (HMF) as redox mediator in solution. Fig. 4C displays the cyclic voltammetric response of the biosensor in the absence (curve a) and in the presence of 5 mM of glucose (curve b) in contact with a 0.1 M pH 7.0 phosphate buffer solution containing 1.0 mM HMF. In this case, the enzyme catalyzes the oxidation of glucose to gluconolactone, while the electrons involved in the process are immediately transferred to the oxidized form of the soluble redox mediator (HMF), regenerating the enzyme activity. The re-oxidation of HMF on the electrode surface leads to a bioelectrocatalytic response that can be observed in curve b, which is proportional to the amount of glucose present in the solution. The process is as follows:

$$\text{Glucose} + (\text{GOx})_{ox} \rightarrow \text{Gluconolactone} + (\text{GOx})_{red}$$

$$(\text{GOx})_{red} + (\text{HMF})_{ox} \rightarrow (\text{GOx})_{ox} + (\text{HMF})_{red}$$

$$(\text{HMF})_{red} - 1e^- \rightarrow (\text{HMF})_{ox}$$

To confirm the role of DNPs in this catalytic response, the cyclic voltammogram of GOx/Au system under the same experimental conditions (Fig. 4D) in absence (curve a) and in presence of glucose (curve b) was obtained. As can be observed, upon addition of glucose, no catalytic waves were observed. The presence of DNPs, besides increasing the relative surface area, can contribute to a better distribution of the enzyme on the surface and promote the electron transfer between the enzyme and the redox mediator, which results in a good bioelectrocatalytic response in the presence of glucose.

3.4. Development of a lactate based diamond nanoparticles modified gold electrode

Once the applicability of DNPs to the development of glucose based biosensors was demonstrated, we extended it to other redox enzymes of interest. In particular, we have prepared a new biosensor based on the same procedure but employing the enzyme lactate oxidase. To our knowledge, this is the first electrochemical biosensor for lactate determination that includes DNPs as nanomaterial. In this case, the response is based on the oxidation of L-lactate to pyruvate, catalyzed by LOx, in presence of HMF. Fig. 5A depicts the cyclic voltammetric response for LOx/DNPs/Au in the absence (curve a) and in the presence of increasing concentrations of lactate (curves b–e) in 0.1 M pH 7.0 phosphate buffer solution containing 1.0 mM HMF.

The analytical properties (linear concentration range, sensitivity, detection limit, reproducibility and repeatability) are obtained. As shown in the inset of Fig. 5B, the calibration plot was linear from 0.05 mM to 0.7 mM concentration range ($r^2 = 0.996$). The sensitivity, calculated from the slope of the plot, was 4.0 μA mM^{-1}. The detection limit, calculated as the ratio between three times the standard deviation of background current and the sensitivity, was 0.015 mM. As can be observed in Table S1, this detection limit compares well with those obtained by others methods commonly employed for lactate determination, such as the enzymatic ones. The repeatability was evaluated from the relative standard deviation (RSD) of nine different measurements of a 5 mM lactate concentration with the same biosensor. A RSD value of 5% was obtained. The reproducibility using four different biosensors was 6%. The storage stability was evaluated, concluding that the biosensor retains 50% of its initial response after 15 days. Finally, we have studied the influence of potential interferents on the lactate biosensor response. In this sense, we have obtained the biosensor response to 0.7 mM of lactate in absence and presence of acetaminophen (0.1 mM), ascorbic acid (0.1 mM) and uric acid (0.1 mM). While the presence of acetaminophen and uric acid has a negligible effect on the biosensor response, addition of ascorbic acid (easily oxidized at electrodes) results in an increase of the catalytic current of 5%. These data suggest that the developed device can be successfully used to measure lactate concentrations

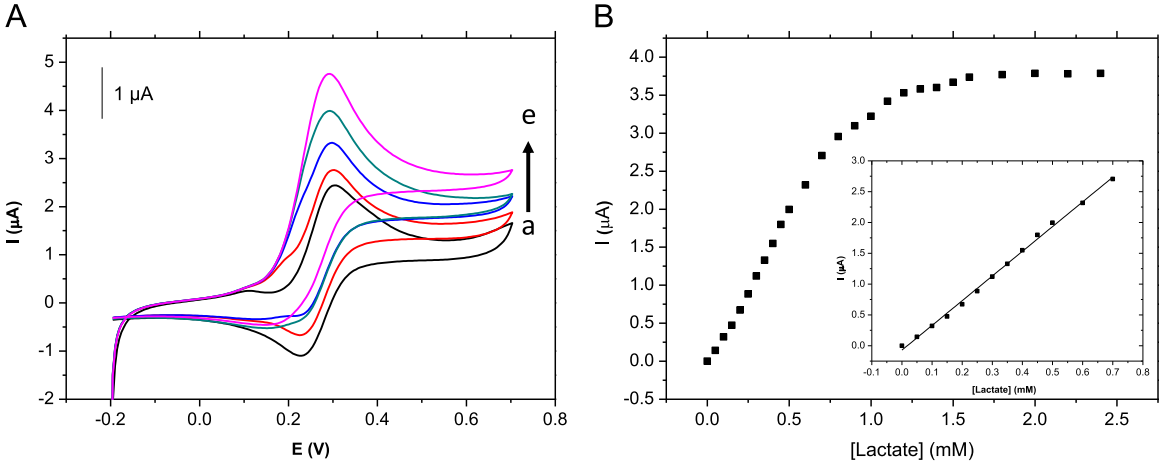

Fig. 5. (A) Cyclic voltammetric response for LOx/DNPs/Au biosensor in contact with a 0.1 M phosphate buffer solution pH 7.0 containing 1.0 mM HMF in absence (curve a) and in presence of 0.1 mM, 0.25 mM, 0.4 mM and 0.6 mM of lactate (curves b–e). Scan rate $\nu = 0.01$ V/s. (B) Calibration curve obtained from these cyclic voltammetric measurements. The inset shows the linear concentration range.

in presence of possible interfering substances.

From these results, it can be concluded that the employment for the first time of diamond nanoparticles as nanomaterial for lactate biosensor fabrication allows obtaining an analytical response which compares well with those obtained for other lactate-based biosensors developed in our laboratory that also include nanomaterials (Casero et al., 2013, 2014; Parra-Alfambra et al., 2011). Moreover, the biosensor developed in the present work shows several advantages such as an easier fabrication procedure and the employment of a less expensive nanomaterial.

4. Conclusions

In the present work, we have demonstrated the suitability of employing undoped diamond nanoparticles (DNPs) as a low cost nanomaterial for developing electrochemical enzyme biosensors, selecting glucose oxidase as a model enzyme. DNPs show a great tendency to aggregate giving rise to a relative large surface roughness (12 nm) when they are deposited onto a gold surface. The resulting DNPs/Au electrode shows electrochemical activity due to the presence of functionalities with unsaturated bonding on the DNPs surface. Both the DNPs/Au and the GOx/DNPs/Au platforms were characterized by AFM, FE-SEM and CV techniques. Since DNPs and GOx have a quite similar size, it is difficult to distinguish them by AFM. Then, in order to sample their differences, force curve measurements were performed allowing to determine an enzyme layer thickness ranging from 9.5 nm to 18 nm. GOx/DNPs/Au shows a clear electrocatalytic response towards glucose oxidation. Once the prototype system was stablished, a new biosensor based on the same approach and lactate oxidase was fabricated (LOx/DNPs/Au), showing a linear concentration range from 0.05 mM to 0.7 mM, a sensitivity of 4.0 μA mM^{-1}, a detection limit of 15 μM and a good reproducibility (RSD 6%).

Acknowledgments

This work has been supported by Ministerio de Ciencia e Innovacion (Project no. CTQ2011-28157), Ministerio de Economía y Competitividad (Project no. FIS2012-38866-C05-05) and Comunidad Autónoma de Madrid (Project NANOAVANSENS S2013/MIT-3029).

Appendix A. Supplementary material

Supplementary data associated with this article can be found in the online version at http://dx.doi.org/10.1016/j.bios.2015.01.044.

References

Barbadillo, M., Casero, E., Petit-Domínguez, M.D., Vázquez, L., Pariente, F., Lorenzo, E., 2009. Talanta 80, 797–802.
Casero, E., Alonso, C., Vázquez, L., Petit-Domínguez, M.D., Parra-Alfambra, A.M., de la., Merino, Fuente M., Álvarez-García, P., Andrés, S., de, Pariente, A., Lorenzo, E., F., 2013. Electroanalysis 25, 154–165.
Casero, E., Alonso, C., Petit-Domínguez, M.D., Vázquez, L., Parra-Alfambra, A.M., Merino, P., Álvarez-García, S., Andrés, A., de., Suárez, E., Pariente, F., Lorenzo, E., 2014. Microchim. Acta 181, 79–87.
Chang, H.C., Lora Huang, L.C., 2004. Langmuir 20, 5879–5884.
Chang, H.C., Nguyen, T.T.B., Wu, V.W.K., 2007. Diam. Relat. Mater. 16, 872–876.
Clark, C.D., Dean, P.J., Harris, P.V., 1964. Proc. R. Soc. Lond. 277, 312–329.
Cunci, L., Cabrera, C.R., 2011. Electrochem. Solid State Lett. 14, K17–K19.
Gaillard, C., Girarnd, H.A., Falck, C., Paget, V., Simic, V., Ugolin, N., Bergonzo, P., Chevillard, S., Arnault, J.C., 2014. RSC Adv. 4, 3566–3572.
Holt, K.B., Caruana, D.J., Millán-Barrios, E.J., 2009. J. Am. Chem. Soc. 131, 11272–11273.
Holt, K.B., 2010. Phys. Chem. Chem. Phys. C 12, 2048–2058.
Kochmann, S., Hirsch, T., Wolfbeis, O.S., 2012. Trends Anal. Chem. 39, 87–113.
Krüger, A., Kataoka, F., Ozawa, M., Fujino, T., Suzuki, Y., Aleksenskii, A.E., Vul', Ya A., Osawa, E., 2005. Carbon 43, 1722–1730.
Kulakova, I.I., 2004. Phys. Solid State 46, 621–628.
Li, J., Zhu, Y., Li, W., Zhang, X., Peng, Y., Huang, Q., 2010. Biomaterials 31, 8410–8418.
Man, H.B., Ho, D., 2012. Phys. Status Solidi A: Appl. Mater. 209, 1609–1618.
Merkoçi, A., Pumera, M., Llopis, X., Pérez, B., del Valle, M., Alegret, S., 2005. Trends Anal. Chem. 24, 826–838.
Nicolau, E., Méndez, J., Fonseca, J.J., Griebenow, K., Cabrera, C.R., 2012. Bioelectrochemistry 85, 1–6.
Novoselova, I.A., Fedoryshena, E.N., Panov, E.V., Bochechka, A.A., Romanko, L.A., 2004. Phys. Solid State 46, 748–750.
Parra, A., Casero, E., Vázquez, L., Pariente, F., Lorenzo, E., 2006. Anal. Chim. Acta 555, 308–315.
Parra-Alfambra, A.M., Casero, E., Petit-Domínguez, M.D., Barbadillo, M., Pariente, F., Vázquez, L., Lorenzo, E., 2011. Analyst 136, 340–347.
Pumera, M., 2009. Chem. Rec. 9, 211–223.
Puzyr, A.P., Baron, A.V., Purtov, K.V., Bortnikov, E.V., Skobelev, N.N., Mogilnaya, O.A., Bondar, V.S., 2007. Diam. Relat. Mater. 16, 2124–2128.
Scholz, J., McQuillan, A.J., Holt, K.B., 2011. Chem. Commun. 47, 12140–12142.
Varley, T.S., Hirani, M., Harrinson, G., Holt, K.B., 2014. Faraday Discuss. 172, 349–364.
Wang, H.D., Yang, Q., Hui Niu, C., Badea, I., 2011. Diam. Relat. Mater. 20, 1193–1198.
Yang, W., Ratinac, K.R., Ringer, S.P., Thordarson, P., Gooding, J.J., Braet, F., 2010. Angew. Chem. Int. Ed. 49, 2114–2138.
Zhang, W., Patel, K., Schexnider, A., Banu, S., Radadia, A.D., 2014. ACS Nano 8, 1419–1428.
Zhao, W., Xu, J.J., Qiu, Q.Q., Chen, H.Y., 2006. Biosens. Bioelectron. 22, 649–655.
Zhu, J.T., Shi, C.G., Xu, J.-J., Chen, H.Y., 2007. Bioelectrochemistry 71, 243–248.